


**Nitrides** Hot Paper
How to cite: *Angew. Chem. Int. Ed.* **2022**, *61*, e202114191

International Edition: doi.org/10.1002/anie.202114191

German Edition: doi.org/10.1002/ange.202114191

# Single-Bonded Cubic AsN from High-Pressure and High-Temperature Chemical Reactivity of Arsenic and Nitrogen

Matteo Ceppatelli,\* Demetrio Scelta, Manuel Serrano-Ruiz, Kamil Dziubek, Marta Morana, Volodymyr Svitlyk, Gaston Garbarino, Tomasz Poręba, Mohamed Mezouar, Maurizio Peruzzini, and Roberto Bini

**Abstract:** Chemical reactivity between As and N<sub>2</sub>, leading to the synthesis of crystalline arsenic nitride, is here reported under high pressure and high temperature conditions generated by laser heating in a diamond anvil cell. Single-crystal synchrotron X-ray diffraction at different pressures between 30 and 40 GPa provides evidence for the synthesis of a covalent compound of AsN stoichiometry, crystallizing in a cubic P2<sub>1</sub>3 space group, in which each of the two elements is single-bonded to three atoms of the other and hosts an electron lone pair, in a tetrahedral anisotropic coordination. The identification of characteristic structural motifs highlights the key role played by the directional repulsive interactions between non-bonding electron lone pairs in the formation of the AsN structure. Additional data indicate the existence of AsN at room temperature from 9.8 up to 50 GPa. Implications concern fundamental aspects of pnictogens chemistry and the synthesis of innovative advanced materials.

## Introduction

Nitrogen and arsenic are the first and the third element of Group 15 of the periodic table, whose members, named pnictogens, have  $ns^2np^3$  outer shell electronic orbital configuration. N and As combine with metal and non-metal elements to form binary and ternary compounds,<sup>[1]</sup> which are of extreme interest for a variety of energy and technology related applications.<sup>[2,3]</sup> They are also known to combine with P, the second element in group 15, forming binary compounds:  $\alpha$ -P<sub>3</sub>N<sub>5</sub>,<sup>[4]</sup>  $\gamma$ -P<sub>3</sub>N<sub>5</sub><sup>[5]</sup> in the case of N and As<sub>x</sub>P<sub>1-x</sub><sup>[6]</sup> in the case of As. Nevertheless, excluding the unstable and highly explosive As(N<sub>3</sub>)<sub>3</sub><sup>[7-9]</sup> and As(N<sub>3</sub>)<sub>5</sub><sup>[10]</sup> molecular azides,

no extended covalent compound entirely made of As and N has ever been reported so far.<sup>[2,11,12]</sup> Even including other elements, the compounds formed by As and N are limited to few elusive and poorly characterized complex ionic units<sup>[13,14]</sup> and covalent oligomeric structures.<sup>[15]</sup>

At ambient conditions As and N<sub>2</sub> do not react spontaneously. Like generally occurring in nitrides synthesis, the high stability of the N≡N triple bond (945 kJ mol<sup>-1</sup>) along the room T isotherm up to at least 100 GPa mostly prevents the direct uncatalyzed chemical reactivity of the N<sub>2</sub> molecule with other systems,<sup>[12,16]</sup> requiring challenging synthesis conditions for the direct nitridation reaction.<sup>[3,17,18]</sup> As a result, the direct chemistry of As and N has remained essentially unexplored.

In the last two decades, high pressure, in combination with electronic photoexcitation<sup>[19,20]</sup> or high temperature conditions,<sup>[21]</sup> has emerged as a powerful tool to overcome energetic barriers and access unexplored reactions paths in otherwise stable pure and multi-component systems, leading to the synthesis of new materials.<sup>[22]</sup> Taking advantage of the high density conditions generated by diamond anvil cells (DACs) and high temperature-quenching rate inherent to laser heating technique, this approach has dramatically changed the idea of the stability and inertness of the N<sub>2</sub> molecule, expanding our knowledge about the chemistry of N and revealing the existence of an entire new class of N-rich materials recoverable at room T on decompression to low or even ambient pressure.<sup>[23-27]</sup>

These experimental evidences nicely fit with recent studies<sup>[2,17,28]</sup> which have explored new compositional spaces for crystalline inorganic nitrides, suggesting the existence of a large variety of compounds to be discovered and identifying



[\*] M. Ceppatelli, D. Scelta, K. Dziubek, R. Bini  
 LENS, European Laboratory for Non-linear Spectroscopy  
 Via N. Carrara 1, I-50019 Sesto Fiorentino, Firenze (Italy)  
 E-mail: ceppa@lens.unifi.it


M. Ceppatelli, D. Scelta, M. Serrano-Ruiz, K. Dziubek, M. Peruzzini, R. Bini  
 ICCOM-CNR, Institute of Chemistry of OrganoMetallic Compounds, National Research Council of (Italy)  
 Via Madonna del Piano 10, I-50019 Sesto Fiorentino, Firenze (Italy)  
 E-mail: matteo.ceppatelli@iccom.cnr.it

M. Morana  
 Department of Chemistry and INSTM, University of Pavia  
 Via Taramelli 16, 27100, Pavia (Italy)

V. Svitlyk, G. Garbarino, T. Poręba, M. Mezouar  
 ESRF, European Synchrotron Radiation Facility  
 71 Avenue des Martyrs, CS40220, 38043 Grenoble Cedex 9 (France)

R. Bini  
 Dipartimento di Chimica "Ugo Schiff" dell'Università degli Studi di Firenze  
 Via della Lastruccia 3, I-50019 Sesto Fiorentino, Firenze (Italy)

 Supporting information and the ORCID identification number(s) for the author(s) of this article can be found under:  
 <https://doi.org/10.1002/anie.202114191>

 © 2021 The Authors. Angewandte Chemie International Edition published by Wiley-VCH GmbH. This is an open access article under the terms of the Creative Commons Attribution Non-Commercial NoDerivs License, which permits use and distribution in any medium, provided the original work is properly cited, the use is non-commercial and no modifications or adaptations are made.

them as ideal candidates to be potentially recovered at ambient conditions as thermodynamically metastable materials. Indeed, according to the thermodynamic scale of metastability for crystalline inorganic materials proposed by Sun et al.,<sup>[28]</sup> nitrides feature the highest enthalpy above the ground state (at 0 K and zero pressure) and the highest cohesive energy among chalcogenides, pnictides and halides. In particular, the ability of forming strong localized covalent bonds with low ionic character can lock the stabilization of high energy structures against unfavorable atomic arrangements, preventing their decomposition or their transformation to the ground state polymorph, and likely allowing the recovery at ambient conditions of new thermodynamically metastable nitrides of relevant technological interest.<sup>[2,28]</sup>

As and N behave very differently at high pressure. The thermodynamically stable allotrope of arsenic is the layered crystalline grey form (As-I,  $A7$ ,  $R\bar{3}m$ ,  $Z=2$ ), structurally analogous to high pressure rhombohedral  $A7$  phosphorus (4.8–10.5 GPa, 298 K), and to ambient pressure Sb-I and Bi-I.<sup>[29]</sup> On increasing pressure along the room T isotherm As-I remains stable up to  $25 \pm 1$  GPa, where it converts to simple cubic (sc) As-II<sup>[30]</sup> (another study locates the As-I to As-II phase transitions at 32 GPa<sup>[31]</sup>). At  $48 \pm 11$  GPa As-II sluggishly transforms into As-III,<sup>[32]</sup> identified as an incommensurately modulated structure<sup>[33]</sup> and at  $97 \pm 14$  GPa As-III ultimately transforms into As-IV (bcc), which is then observed up to highest investigated pressure of 122 GPa.<sup>[32]</sup>

Nitrogen, on the other side, forms a diatomic molecule at ambient conditions, which, after condensation and solidification at 2.4 GPa, persists over a wide range of pressure and temperature conditions up to about 100 GPa, through the  $\beta$ ,  $\delta$ ,  $\delta_{\text{loc}}$ ,  $\epsilon$ , and  $\zeta$  molecular crystalline structures.<sup>[34]</sup> Between 100 and 150 GPa a sufficiently high density is achieved to perturb the  $N_2$  molecular structure and N is reported to amorphize.<sup>[35]</sup> Laser heating (LH) in these conditions leads to the synthesis of polymeric single bonded structures like cubic-gauche N (cg-N, 110 GPa and 2000 K),<sup>[23]</sup> layered polymeric N (LP-N,  $Pba2$ , above 125 GPa and 2000 K),<sup>[36]</sup> hexagonal layered polymeric N (HLP-N,  $P4_2bc$ , 240 GPa and 3300 K)<sup>[37]</sup> and, as recently reported, to a layered crystalline structure analogous to the orthorhombic black phosphorus (140 GPa, 4000 K<sup>[24]</sup> and 146 GPa, 2200 K<sup>[25]</sup>), thus extending to N the structural consistency and similarities highlighted by pressure for heavier pnictogens.<sup>[29]</sup>

In this paper we used synchrotron X-ray diffraction (XRD) to explore the occurrence of chemical reactivity between As and molecular  $N_2$  under high pressure and high temperature conditions, generated by means of laser heated diamond anvil cell. According to this approach, which has been recently applied in successfully activating the formation of chemical bonds between lighter pnictogen P and molecular  $H_2$ ,<sup>[21]</sup> As is used as a reactant and laser absorber, while  $N_2$  is employed as a reactant and pressure transmitting medium, thus avoiding the presence of any precursor, catalyst, or contaminant.

The investigation of the chemical reactivity between As and N under extreme pressure and temperature conditions is not only important to address specific issues about fundamental pnictogens chemistry but is currently relevant to the

possibility of taking advantage of pressure to design and synthesize innovative materials of energetic and technological relevance, potentially recoverable at ambient conditions in their stable or metastable states, as suggested by theoretical indications. Examples include nitrides,<sup>[2,28]</sup> N-doped arsenene based materials,<sup>[38–41]</sup> high energy density materials<sup>[23]</sup> and advanced thermoelectrics.<sup>[42]</sup>

## Results and Discussion

After loading the sample of As and  $N_2$  into the DAC (SI-1 Experimental Section), XRD patterns were acquired at several pressure points during room T compression, while monitoring the evolution with pressure of the As and N structures. Laser heating at 14.7 GPa (1050–1400 K, 1064 nm, 15–20 W) did not produce any chemical change of the sample, with all the peaks in the room T diffraction pattern consistently assigned to the As-I and  $\delta$ - $N_2$  phases.

Reactivity between arsenic and nitrogen was instead observed during two independent laser heating experiments at 25.0 GPa and 36.0 GPa, in which a full XRD mapping of the sample (5  $\mu\text{m}$  spatial resolution), performed at room T after LH (Figure SI-2 and Figure SI-3), revealed the presence of single crystal domains from an unknown crystal structure not compatible with any known phase of arsenic and nitrogen at similar thermodynamic conditions. The occurrence of chemical reactivity is also evidenced by the appearance of new diffraction peaks, in addition to those expected for  $N_2$  and As, in panoramic XRD acquisitions collected in the laser heated area of the sample at room T after LH (Figure 1).

The indexing of the new structure provided a primitive cubic unit cell, while the integrated space-group and crystal-structure determination indicated the  $P2_13$  symmetry ( $Z=32$ ), with AsN stoichiometry and eight symmetry independent atoms in the asymmetric unit: two As and two N atoms in  $12b$  sites, and other two As and two N atoms in  $4a$  sites. Salient structure refinement parameters regarding one of the best-quality dataset acquired at 35.6 GPa are shown in Table 1, whereas those regarding different pressure points are reported in Table SI-1.

AsN single crystal data were collected and refined between 27.2 and 38.6 GPa, however the detection of the most intense diffraction peaks in the panoramic XRD acquisitions indicated the persistence of polycrystalline cubic AsN at room T up to ca. 50 GPa on compression and down to 9.8 GPa on decompression, suggesting the possibility to recover this product at ambient conditions. Above 50 GPa the missed detection of AsN coincided with the transition of simple cubic As-II to incommensurate As-III. No phase transition of AsN was detected in the 9.8–50 GPa pressure range. The unit cell volume of the AsN sample synthesized at 36.0 GPa, obtained from single crystal refinement, is plotted as a function of pressure in Figure 2A (additional data are reported in Figure SI-10). The limited pressure interval of the acquired data and the absence of data near ambient pressure did not allow a reliable convergence of the data fit to extract the bulk modulus of AsN using either a Vinet or a third order Birch-Murnaghan equations of state. Nevertheless, a qualita-

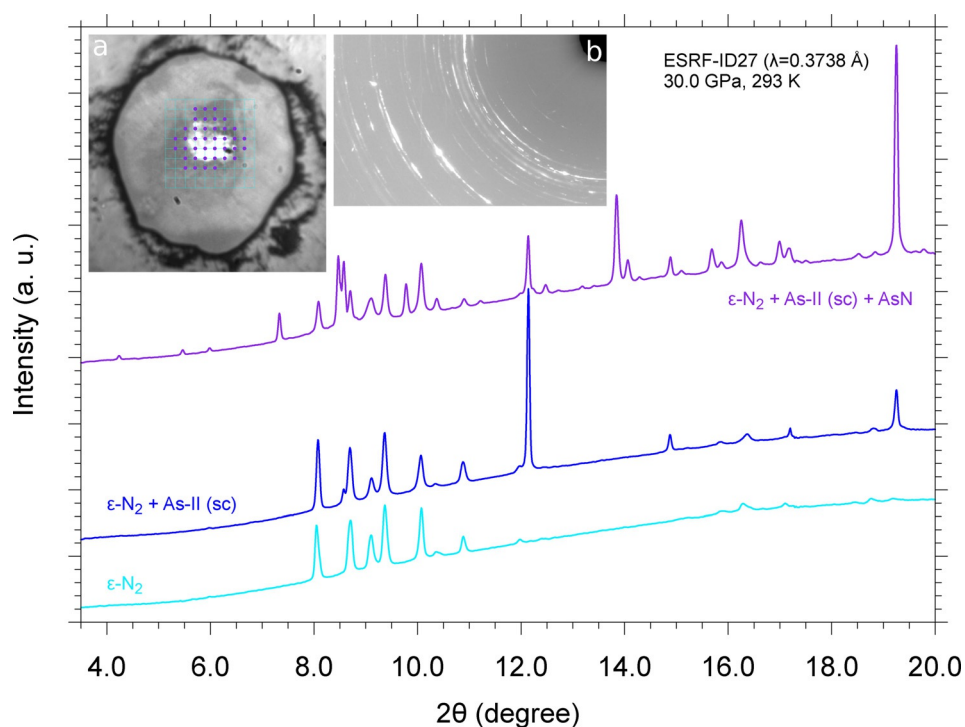


**Figure 1.** Selected integrated XRD patterns corresponding to panoramic acquisitions at room T and 30 GPa on different points of the sample laser heated at 25.0 GPa. The patterns were acquired in the points of the grid superimposed to the sample image (a), which shows a shining area at the center, corresponding to the original piece of As (As-II, sc), surrounded by N<sub>2</sub> ( $\epsilon$ -N<sub>2</sub>). The violet full circles on the grid indicate the points of the sample where the reaction product AsN was detected (violet upper trace), whereas the unlabeled points on the outer part of the grid indicate the sample points where only  $\epsilon$ -N<sub>2</sub> (cyan lower trace) or only  $\epsilon$ -N<sub>2</sub> and sc-As (blue middle trace) were observed. A portion of a detector image, acquired in one of the violet points of the grid, is shown in (b).

**Table 1:** Selected refinement parameters for the crystal structure of AsN at 35.6 GPa and room temperature.<sup>[a]</sup>

Chemical formula	AsN
Pressure [GPa]	35.6
Temperature [K]	293
Crystalline system	Cubic
Space group	$P2_13$ (n. 198)
$a$ [Å]	8.7024(4)
$V$ [Å <sup>3</sup> ]	659.06(10)
$Z$	32
density [g cm <sup>-3</sup> ]	7.170
Wavelength [Å]	0.41047
No. of $m/i/o$ [ $I > 2\sigma(I)$ ] reflections	1605, 804, 650
$R_{int}$	0.023
Final $R$ indices [ $I > 2\sigma(I)$ ]	$R1 = 0.040$ , $wR2 = 0.082$
Final $R$ indices [all data]	$R1 = 0.053$ , $wR2 = 0.086$
$S$ (goodness of fit)	0.982
No. of parameters	49

[a]  $m$ ,  $i$ ,  $o$ , respectively indicate measured, independent, and observed reflections.

tive insight about the bulk modulus of AsN can be obtained by comparing the evolution with pressure of the volume of AsN, normalized to its value at 9.8 GPa (the lowest pressure where it could be detected), to the evolution with pressure of the volume of N<sub>2</sub> ( $\delta$ -N<sub>2</sub> and  $\epsilon$ -N<sub>2</sub>),<sup>[43,44]</sup> As (As-I, As-II and As-

III)<sup>[30,45]</sup> and  $cg$ -N,<sup>[23]</sup> normalized to the volume of their corresponding stable phases at room T and 9.8 GPa. The comparison indicates that in the investigated pressure range AsN is more compressible than covalent single bonded  $cg$ -N, but less compressible than As-I, As-II and possibly As-III (Figure 2B).

To our best knowledge, no other experimentally synthesized binary nitride is known to adopt this intriguing complex structure, which has been reported for just a few compounds: yellow  $\alpha$ -indium (I) chloride InCl,<sup>[46–49]</sup>  $\pi$ -cubic tin (II) sulfide SnS,<sup>[50]</sup> and intermetallic phases strontium aluminide SrAl<sup>[51,52]</sup> and strontium gallide SrGa.<sup>[51]</sup> The atomic/ionic arrangement in these materials resembles a severely distorted rocksalt (B1) structure, with the  $P2_13$  phase lattice parameter twice as large as that of the underlying  $Fm\bar{3}m$  structure and four types of cation and anion, respectively.

In our structure determinations, the As–N bonding distances vary between 1.842(9) Å and 1.923(13) Å (Table SI-2 and Figure SI-4), in a good agreement with an average ambient pressure value for the As–N single bond length of 1.86(3) Å, as derived from a statistical survey of the Cambridge Structural Database (CSD).<sup>[53]</sup>

On the other hand, the shortest interatomic As $\cdots$ As distances are in the 2.801(2)–2.849(3) Å range (Table SI-2 and Figure SI-4), thus considerably longer than the 2.459(11) Å average As–As covalent bond length recorded in the CSD,<sup>[53]</sup> and than the As–As bond distance of elemental arsenic in the A7 (As-I) structure, both at ambient pressure (2.52 Å) and at 25 GPa (2.48 Å), and in the sc (As-II) structure (2.55 Å) at 25 GPa.<sup>[30]</sup> In addition, the shortest N $\cdots$ N distances in AsN are more than 1 Å longer than the typical N–N single bond length, which does not exceed 1.46 Å at ambient pressure,<sup>[53]</sup> excluding also the presence of  $-N=N-$  pernitride units and indicating the complete cleavage of the N $\equiv$ N triple bond. Only As–N bonds are thus involved in the connection scheme. Every As is at the apex of a pyramid, whose base is formed by the three nearest N atoms, and every N is at the apex of a pyramid, whose base is formed by the three nearest As atoms. Each As atom connects to and is shared by three NAs<sub>3</sub> pyramids and vice versa. Accordingly, the crystalline structure of AsN is made of a covalently bonded three-dimensional network of vertex sharing and alternating AsN<sub>3</sub> and NAs<sub>3</sub> trigonal pyramids (Figure 3), in which both

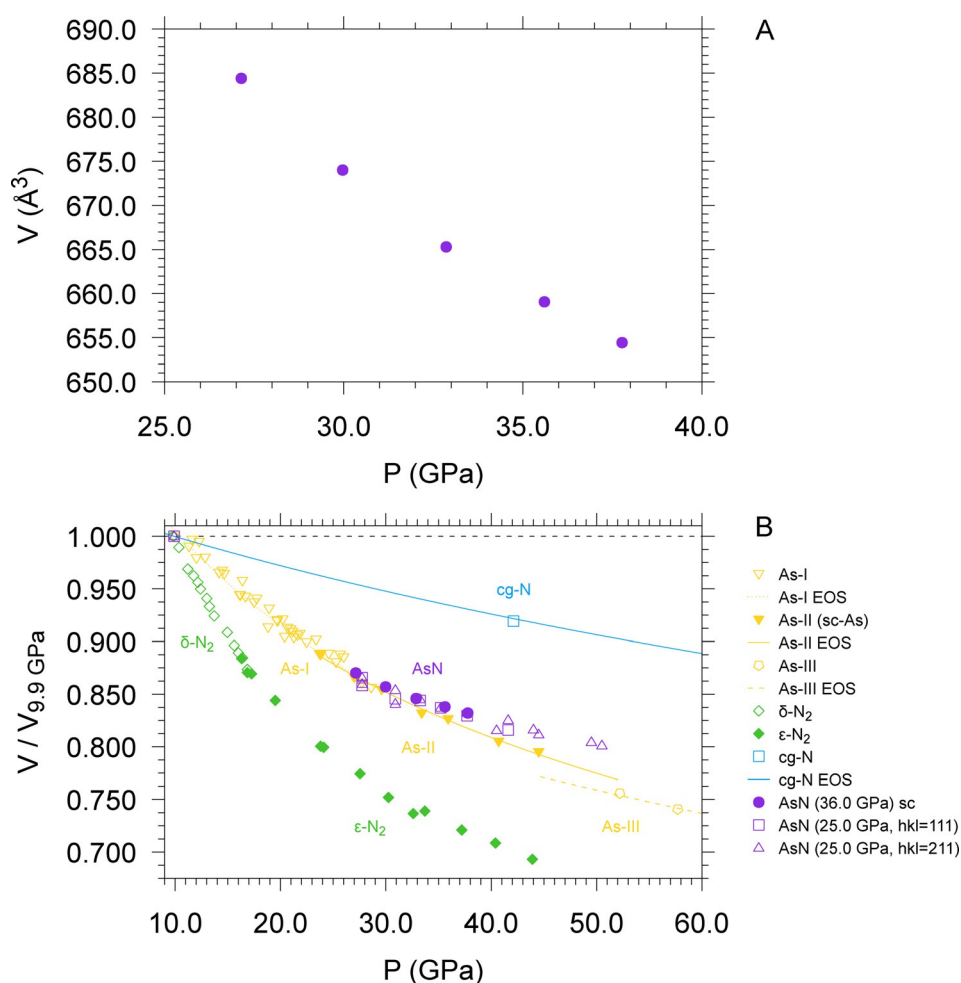


**Figure 2.** A) Evolution with pressure of the unit cell volume of AsN at room T obtained from single crystal data refinement. The plotted data were acquired during the decompression of the sample synthesized at 36.0 GPa. All the pressures were obtained by averaging the values obtained from Au and ruby calibrants. The data point at 38.6 GPa mentioned in the text is not shown here for dataset consistency, due to absence of the Au pressure value for this data point. For the volume corresponding to 27.2 GPa only the unit cell parameters, with no refinement of the atomic positions, could be obtained. B) Evolution with pressure of the unit cell volume of N<sub>2</sub>,<sup>[43]</sup> As,<sup>[30,45]</sup> cg-N<sup>[23]</sup> and AsN, normalized to the volume of their stable phase at room T and 9.8 GPa, corresponding to the lowest pressure at which AsN was observed. For AsN the filled circles correspond to the data plotted in (A), whereas the empty squares and up triangles correspond to data from the sample synthesized at 25.0 GPa, respectively obtained using the 111 and 211 reflections of AsN observed in azimuthally integrated patterns (Figure SI-10). The EOS of As-I, As-II, As-III<sup>[30,45]</sup> and cg-N<sup>[23]</sup> are also plotted.

elements have valence state 3. The presence of three nearest neighbors instead of six, as occurring in a typical octahedral coordination, and the relatively small Pauling electronegativity difference ( $\Delta\chi = 0.86$ ) between As ( $\chi_{\text{As}} = 2.18$ ) and N ( $\chi_{\text{N}} = 3.04$ ), supports the covalent rather than ionic nature of AsN, according to the van Arkel–Ketelaar triangle, which requires  $\Delta\chi > 1.7$  for ionicity in binary compounds.<sup>[54]</sup>

Inspection of the valence angles connecting nearest neighbors indicates that, within the investigated pressure interval, the N-As-N angles are grouped in the 88.9(4)°–99.5(5)° range (Table SI-2 and Figure SI-5). Whereas two of them have  $\leq 90^\circ$  value and one varies with pressure between 98.5° and 99.5°, all the other N-As-N angles range between 90° and 94.2(5)°, in substantial agreement with literature

reports containing trigonal pyramidal systems of trivalent As featuring  $4s^2$  non-spherical asymmetric electron distribution and lone pair expression (Section SI-4). The As-N-As angles are instead grouped between 107.3(6)° and 113.6(4)°, across to the 109.45° value expected for tetrahedrally coordinated N atoms, with only one angle adopting values between 103.4(6)° and 103.8(6)°. Interestingly, the two N-As-N and As-N-As angles, respectively having the highest (98.5° and 99.5°) and the lowest (103.4° and 103.8°) value within the corresponding group, seem to approach each other value, indicating the existence of distortion within some AsN<sub>3</sub> and NAs<sub>3</sub> trigonal pyramids. These findings agree with the known fact that, while the ammonia molecule adopts an almost ideal  $sp^3$  hybridization with a H-N-H angle value of 108°, in other XH<sub>3</sub> hydrides of group 15 elements bond angles of 90°–93° are observed.<sup>[55]</sup> This phenomenon is equally present in other structures with trivalent N and As atoms: for example the angles in arsenic nitride (CCDC refcode: HMA-TAS)<sup>[56]</sup> or 2,4,6,8,9,11-hexaphenyl-2,4,6,8,9,11-hexa-arsa-1,3,5,7,10-penta-azabicyclo-(3.3.3)undecane (CCDC refcode: PASAZD).<sup>[57]</sup>

The  $P2_13$  structure has been computationally predicted to exist at high pressure also in binary single bonded cubic gauche carbon nitride (cg-CN),<sup>[58]</sup> whereas the experimentally high pressure synthesized single bonded cg-N adopts the related  $I2_13$  structure,<sup>[23]</sup> consistently with the presence of only one type of atom. Interestingly, cg-N could be actually regarded as an extremely distorted sc  $\alpha$ -Po type structure. Such distorted cubic structure is instead not observed in As, which adopts an ideal octahedral coordination scheme in sc-As (As-II), exhibiting six equivalent nearest neighbors with all the valence angles equal to 90°. The corresponding  $Fm\bar{3}m$  AsN structure would represent the hypothetical undistorted rock salt structure with six equivalent nearest neighbors and 90° valence angles for both As and N. The connection scheme of AsN is thus different with respect to sc-As due to the



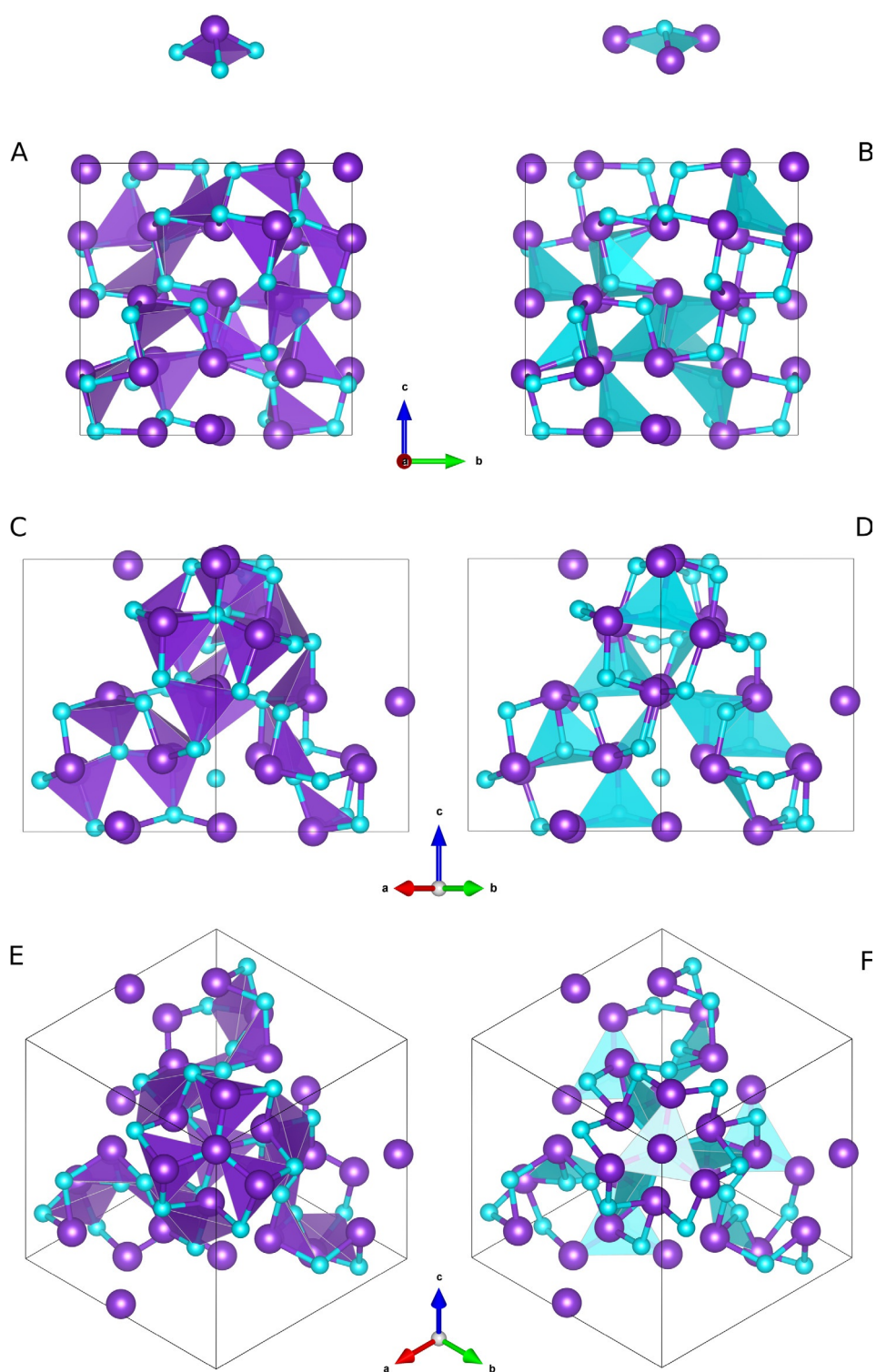


**Figure 3.** Different views of the  $P_{2,3}$  unit cell of AsN (As atoms in violet and N atoms in light blue) in the ball-stick representation mode along different crystallographic directions:  $[100]$  (A and B),  $[110]$  (C and D), one of the  $C_3$  axis directed along  $[111]$  (E and F). The shaded polyhedra indicate the  $AsN_3$  (left) and  $NAs_3$  (right) trigonal pyramids mentioned in the text and highlighted on the top of the Figure. Data refer to AsN at 35.6 GPa and 293 K.

structural frustration stemming from the presence of two distinct atomic species exhibiting different preferences for the coordination geometry. However, the close relationship

in the AsN structure (Figure 3 and Figures SI-11 to SI-13).

Like in the isostructural  $P_{2,3}$  systems,<sup>[48,50]</sup> four types of As and N atoms are present in the AsN unit cell, which we will

between the AsN and cg-N crystal structures is evident, as the first one can be ideally obtained by replacing every nearest neighbor in cg-N with an As atom (Figure 4). This is very different from the phosphorus nitride polymorphs ( $\alpha$ - $P_3N_5$ ,<sup>[4]</sup>  $\gamma$ - $P_3N_5$ ,<sup>[5]</sup>), where the valence adopted by P leads to different stoichiometry, coordination scheme and crystalline structure.

Within the assumption of an electron-precise bonding, according to the electronic orbital configuration of pnictogens and to the valence shell electron pair repulsion (VSEPR) theory, an electron lone pair is expected to be located at each As and N atom perpendicularly to the base of the corresponding trigonal pyramid, occupying the fourth corner in an ideal tetrahedral coordination.<sup>[59]</sup> Such atomic arrangement defines three-dimensional regions of space in the AsN unit cell, where non-bonding electron lone pairs likely interact with dominating repulsive interactions (Figure 3 and 5 and Figures SI-11 to SI-13).

Non-bonding electron lone pairs located at the As and N atoms are thus expected to play a key role in determining the distortion of the AsN cubic structure, by adopting orientations able to minimize the repulsive interactions. As a matter of fact, lone pair expression, intimately related to the degree and extension of covalent bonding, seems to be enhanced by cooperative effects in connected  $XY_3$  units with reduced Y-X-Y angle with respect to the isolated ones, as reported for  $SbX_3$  units.<sup>[60]</sup> Structural motifs typical of systems featuring electron lone pair expression, such as cage-like cavities and channels, with facing electron lone pairs, are indeed present

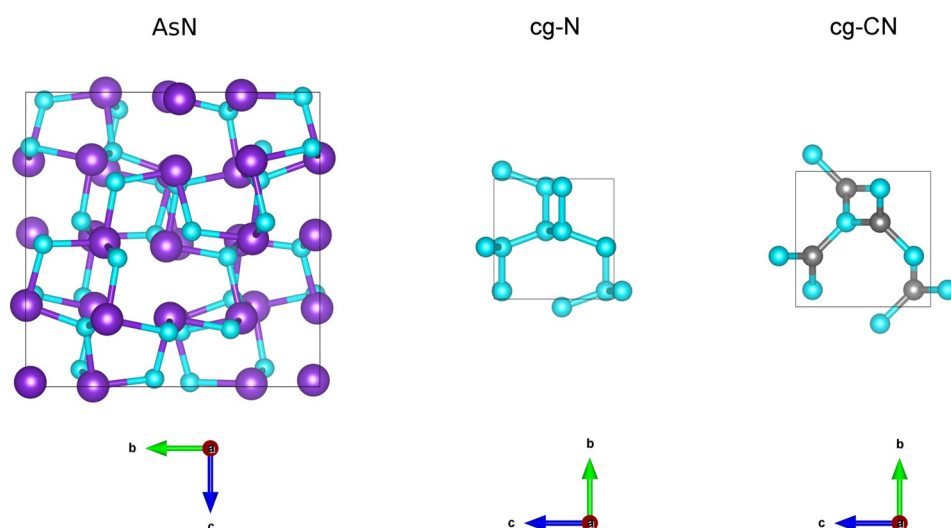


**Figure 4.** Unit cells of binary N-containing compounds with  $P2_13$  structure compared to  $cg-N$  ( $I2_13$ ): AsN (35.6 GPa, 293 K,  $a = 8.7024 \text{ \AA}$ ,  $V = 659.05 \text{ \AA}^3$ ,  $P2_13$ ,  $Z = 32$ ),  $cg-N$  (115 GPa, 300 K,  $a = 3.4542 \text{ \AA}$ ,  $V = 41.214 \text{ \AA}^3$ ,  $I2_13$ ,  $Z = 8$ ),<sup>[23]</sup>  $cg-CN$  (12.7–36.4 GPa, 0 K,  $a = 3.936 \text{ \AA}$ ,  $V = 60.98 \text{ \AA}^3$  at ambient P,  $P2_13$ ,  $Z = 4$ ).<sup>[58]</sup> The size of the unit cells is scaled relatively to their real size. As violet, N light blue, C gray.

refer to in the text, figures and SI using progressive numbers (As or N 01,02,03,04) corresponding to the associated cif file.<sup>[73]</sup>

A chemical inspection at the AsN structure leads to the discovery of four different types of approximately tetrahedral  $As_4$  units, involving different types of As atoms. The four  $As_4$  tetrahedra ( $As04-As01-As01-As01$ ,  $As03-As02-As02-As02$ ,  $As04-As02-As02-As02$ , and  $As03-As01-As01-As01$ ), are shown in Figure 5 and extensively described in the SI (Section SI-5). Whereas these arrangements closely reminds the ambient pressure  $As_4$  molecular units of yellow arsenic, in which every As atom is connected to the other three and the electron lone pairs located at the vertices of the tetrahedron point outwards, the  $As_4$  atoms forming the tetrahedra observed in AsN are not directly chemically bonded as their interatomic distances ( $> 2.8 \text{ \AA}$ ) exceed the expected As–As bond length at comparable pressure (Table SI-3 and Figure SI-6 to SI-9). Within the covalent connection scheme of AsN, the four As atoms of each tetrahedron are always bridged by at least one N atom. Furthermore, the existence of these  $As_4$  tetrahedra appears to be determined by the relative orientations of the electron lone pairs located at their vertices, which create electron rich density regions pointing inside, outside or around the  $As_4$  tetrahedron. Such high electron density regions are further crowded by the electron lone pairs of the surrounding N atoms. In the four types of  $As_4$  tetrahedra described here the presence and expression of electron lone pairs is fully supported by the pressure behavior of the interatomic distances and angles (Section SI-5).

The presence of cage-like structures made by three condensed six-membered cyclotriarsazene  $As_3N_3$  rings is another characteristic feature, worth to be mentioned, typical of chemical system with electron lone pair expression.<sup>[60]</sup> These structural motifs are particularly evident along the  $C_3$  axes, as displayed in the two examples shown in Figures 5A and 5C, and highlighted in Figure SI-13. In the first example

each ring shares one bond with each of the other two rings around a common central N atom (N04) (Figure 5A and Figure SI-13A and SI-13B), whereas in the second one each ring shares three bonds with each of the other two rings and the three have one As (As03) and one N (N03) common atoms located on the  $C_3$  axis in a sort of adamantane-like  $As_4N_4$  pnictogen equivalent (Figure 5C, Figure SI-13C and SI-13D).

Considering the whole covalent framework of AsN, in which these structural motifs are assembled, it emerges that the minimization of the repulsive energy leads to streams of the electron lone pairs, which can be appreciated along specific directions.

For example, the above mentioned tetrahedra and cages, represented in Figure 5A, 5B and 5C, are repeatedly stacked along each of the  $C_3$  axis of the unit cell. One of these atomic arrangements, coincident with the  $[111]$  direction of the cell diagonal, is shown in Figure 5D and 5E. Along the  $C_3$  axis the electron lone pairs of each successive couple of alternating  $AsN_3$  and  $NAs_3$  pyramid have opposite directions. The pyramids connected to them, which are not lying on the  $C_3$  axis, are symmetry transformed as alternating layers of  $NAs_3$  and  $AsN_3$  pyramids, located on planes perpendicular to  $C_3$  and circularly oriented along opposite directions around the  $C_3$  axis, to minimize the repulsive interactions of their electron lone pairs. The presence of  $3_1$  and  $3_2$  screw axes further determines a sort of helical channels of electron lone pair density across the AsN framework (Figure 3E and 3F and Figure SI-12E and SI-12F).

The connection between structural distortion and electron lone pairs has emerged also in  $P2_13$  isostructural systems, where it has been related to the stereoactivity of the electron lone pairs both in the octahedral coordination scheme of  $\alpha$ - $InCl$ <sup>[48]</sup> and in the quasi-tetrahedral coordination environment of  $\pi$ - $SnS$ .<sup>[50,61,62]</sup> Interestingly, like AsN,  $\pi$ - $SnS$  exhibits three considerably shorter Sn–S bond distances, with the S–Sn–S angles ranging between  $87(6)^\circ$  and  $92(4)^\circ$ , and the Sn–S–Sn ones between  $97(5)^\circ$  and  $106(5)^\circ$ , analogously to the N–As–N and As–N–As angles in AsN, respectively. Lone pair stereoactivity is an electronic effect associated to the mixing of the cation  $s$  and anion  $p$  valence shell orbitals, which generates a high energy antibonding orbital able to interact with the unoccupied  $p$  orbitals of the cation by means of a structural distortion.<sup>[63]</sup> Such interaction allows the formation of a localized electronic state hosting the electron lone pair. This phenomenon is typically observed in cations of the  $p$ -block elements with  $ns^2np^0$  electronic configuration, and is associated to the observation of highly anisotropic atomic coordination.<sup>[2]</sup> Even if very few datasets are available in literature

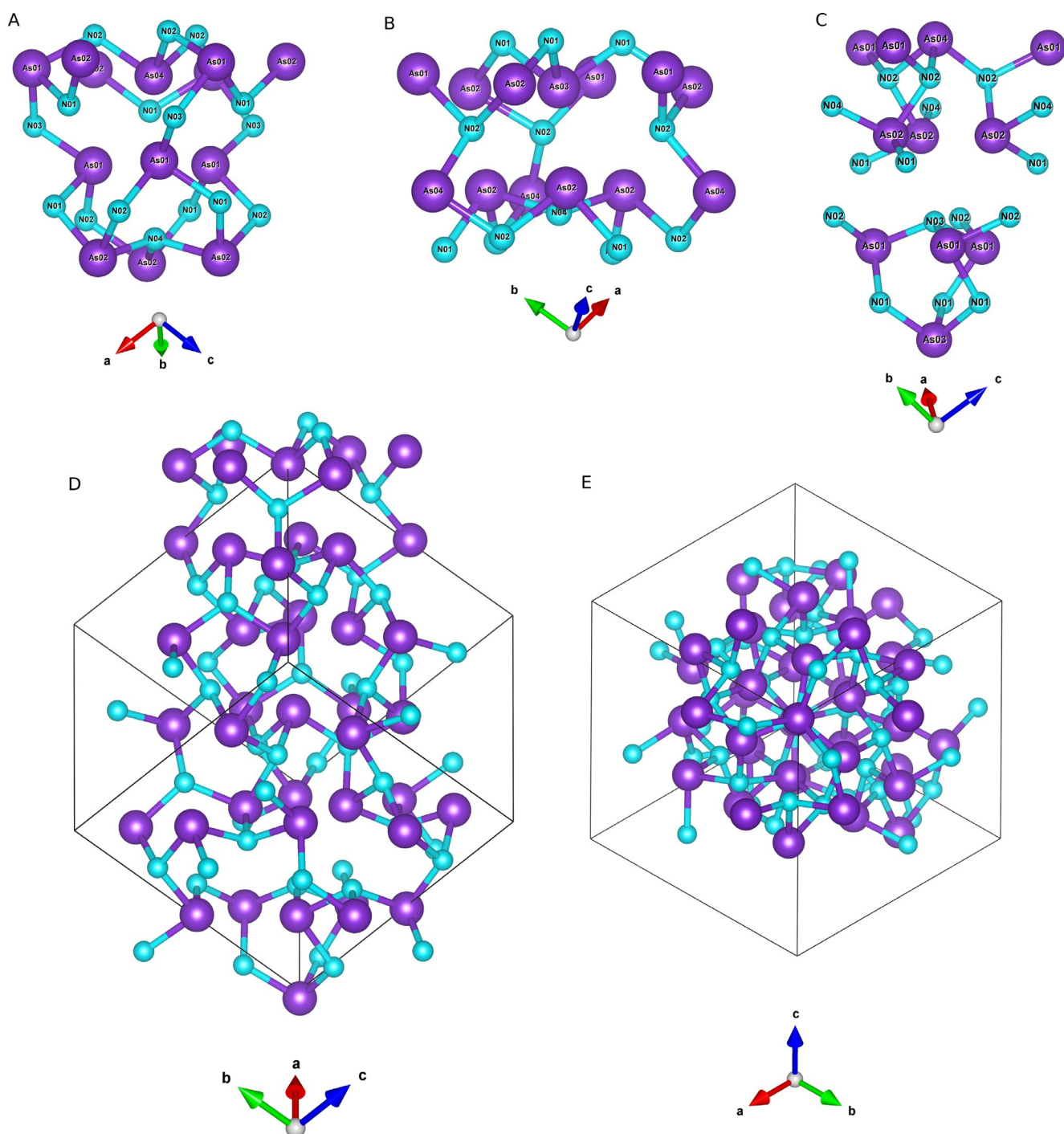


**Figure 5.** Selected regions of the AsN unit cell showing different As<sub>4</sub> cage-like tetrahedral structures: A As<sub>4</sub>-As01-As01-As01, B As<sub>3</sub>-As02-As02-As02, C As<sub>4</sub>-As02-As02-As02 and As<sub>3</sub>-As01-As01-As01. Their arrangement along one of the C<sub>3</sub> axes, coincident with the [111] direction of the cell diagonal, is shown in (D) and (E). The structural motifs shown in this Figure refer to AsN at 35.6 GPa and 293 K.

for stereoactive electron lone pairs in nitrides in general and no information about any compound made of As and N was contained in the analyzed dataset, a recent extensive analysis of structural parameters and valence-bond properties performed by Gagné,<sup>[2]</sup> focused at identifying new compositional spaces for the synthesis of functional inorganic nitrides, has predicted an optimal matching of atomic orbital energy to originate lone pair stereoactivity in AsN. Considering that

lone pair stereoactivity is favored by the higher *s* character of the antibonding orbital, the smaller value of the N-As-N bond angles, compared to the As-N-As ones, indicate for As a higher *p* orbital bonding contribution to the formation of the As–N bonds and a higher *s* character of the corresponding antibonding orbital with respect to N, which is a condition expected to favor orbital mixing and hence lone pair stereoactivity.<sup>[2,60]</sup>



According to the principle of “remnant metastability” proposed by Sun et al.,<sup>[28]</sup> a metastable phase is more likely to be synthesized in its thermodynamic stability range, upon application of specific conditions (pressure, temperature, etc.) and then recovered as metastable outside of it, rather than to be produced directly in its metastable state. In the investigated pressure range and on our experimental time scale, As and N do not react spontaneously at high pressure to form AsN without LH and AsN, once formed, does not transform back into the elements spontaneously. Except for this evidence, indicating the existence of high energetic barriers, the thermodynamic stability vs. metastability of AsN remains an open question, hopefully stimulating further theoretical investigation. Indeed, considering that to our best knowledge no covalent compound of As and N, forming an extended tridimensional framework, has ever been predicted so far by any theoretical study, the experimentally identified crystal structure of AsN reported here certainly represents a challenging benchmark system for computational chemists, in order to accurately describe the localization of the electron lone pairs, their deflection with pressure and their effect on the structural distortion, while providing further insight about the mechanical, thermal and electronic properties of AsN. The presence of electron lone pairs is indeed relevant to important physical properties.<sup>[2]</sup> In particular, together with other features observed in AsN, like the large size of the unit cell and the local static distortion, it has been related to the disruption of lattice heat transport,<sup>[64–66]</sup> by reducing the mean free path of phonons,<sup>[67]</sup> and has been identified among the main targets to achieve ultra-low thermal conductivity and thermoelectric performance,<sup>[68–71]</sup> as recently predicted in 2D puckered  $\alpha$ -arsenene.<sup>[42]</sup> Within this perspective, the synthesis of AsN represents the first step towards the exploration of the high pressure chemistry of As and N, possibly leading to the discovery of other structures and stoichiometries.

## Conclusion

We report here the experimental observation of direct chemical reactivity between As and N under high pressure and high temperature conditions and the synthesis of covalent single-bonded crystalline AsN from the elements according to chemical Equation (1):



While from a chemical point of view the experimental results of this study mark a significant advancement about reactivity and bond theory in pnictogens, providing insights on the chemical interaction between As and N and once again highlighting the key role played by the electron lone pairs in the high pressure chemistry of pnictogens,<sup>[21,29,72]</sup> the discovery and structural characterization of AsN experimentally confirm the theoretical indications for the existence of novel nitrides,<sup>[2,28]</sup> and open new perspectives for the design and high pressure synthesis of advanced As and N based inorganic materials of energetic and technological relevance.

## Acknowledgements

Thanks are expressed to EC through the European Research Council (ERC) for funding the project PHOSFUN “Phosphorene functionalization: a new platform for advanced multifunctional materials” (Grant Agreement No. 670173) through an ERC Advanced Grant. This study was supported by the Deep Carbon Observatory (DCO) initiative under the project *Physics and Chemistry of Carbon at Extreme Conditions*, by the project “GreenPhos - alta pressione”, by the Italian Ministero dell’Istruzione, dell’Università e della Ricerca (MIUR), and by Fondazione Cassa di Risparmio di Firenze under the project HP-PHOTO-CHEM. The authors acknowledge the European Synchrotron Radiation Facility (ESRF) for provision of synchrotron radiation facilities and thank V. Svitlyk, G. Garbarino, M. Mezouar and T. Poręba for assistance in using beamlines ID27 and ID15B (doi 10.1515/ESRF-ES-404440903). Open Access Funding provided by Consiglio Nazionale delle Ricerche within the CRUI-CARE Agreement.

## Conflict of Interest

The authors declare no conflict of interest.

**Keywords:** arsenic nitride · diamond anvil cell · high pressure chemistry · laser heating · X-ray diffraction

- [1] J.-H. Chen, K. H. Whitmire, *Coord. Chem. Rev.* **2018**, 355, 271–327.
- [2] O. C. Gagné, *Chem. Sci.* **2021**, 12, 4599–4622.
- [3] Y. Ma, L. Xiong, Y. Lu, W. Zhu, H. Zhao, Y. Yang, L. Mao, L. Yang, *Front. Chem.* **2021**, 9, 638216.
- [4] S. Horstmann, E. Irran, W. Schnick, *Angew. Chem. Int. Ed. Engl.* **1997**, 36, 1873–1875; *Angew. Chem.* **1997**, 109, 1938–1940.
- [5] K. Landskron, H. Huppertz, J. Senker, W. Schnick, *Angew. Chem. Int. Ed.* **2001**, 40, 2643–2645; *Angew. Chem.* **2001**, 113, 2713–2716.
- [6] I. Shirovani, J. Mikami, T. Adachi, Y. Katayama, K. Tsuji, H. Kawamura, O. Shimomura, T. Nakajima, *Phys. Rev. B* **1994**, 50, 16274–16278.
- [7] T. M. Klapötke, P. Geissler, *J. Chem. Soc. Dalton Trans.* **1995**, 3365–3366.
- [8] R. Haiges, A. Vij, J. A. Boatz, S. Schneider, T. Schroer, M. Gerken, K. O. Christe, *Chem. Eur. J.* **2004**, 10, 508–517.
- [9] Z. Xiaoqing, W. Weigang, L. Fengyi, G. Maofa, S. Zheng, W. Dianxun, *Eur. J. Inorg. Chem.* **2006**, 416–421.
- [10] R. Haiges, J. A. Boatz, A. Vij, V. Vij, M. Gerken, S. Schneider, T. Schroer, M. Yousufuddin, K. O. Christe, *Angew. Chem. Int. Ed.* **2004**, 43, 6676–6680; *Angew. Chem.* **2004**, 116, 6844–6848.
- [11] D. H. Gregory, *J. Chem. Soc. Dalton Trans.* **1999**, 259–270.
- [12] E. Kroke, *Angew. Chem. Int. Ed.* **2002**, 41, 77–82; *Angew. Chem.* **2002**, 114, 81–86.
- [13] A. Schulz, A. Villinger, *Angew. Chem. Int. Ed.* **2008**, 47, 603–606; *Angew. Chem.* **2008**, 120, 614–617.
- [14] A. Schulz, A. Villinger, *Inorg. Chem.* **2009**, 48, 7359–7367.
- [15] G. Schmid, K. Hättmann, *Adv. Mater.* **1996**, 8, 484–486.
- [16] W. Schnick, *Angew. Chem. Int. Ed. Engl.* **1993**, 32, 806–818; *Angew. Chem.* **1993**, 105, 846–858.
- [17] W. Sun, A. Holder, B. Orvananos, E. Arca, A. Zakutayev, S. Lany, G. Ceder, *Chem. Mater.* **2017**, 29, 6936–6946.



- [18] T. M. M. Richter, R. Niewa, *Inorganics* **2014**, *2*, 29–78.
- [19] M. Ceppatelli, R. Bini, V. Schettino, *Proc. Natl. Acad. Sci. USA* **2009**, *106*, 11454–11459.
- [20] M. Ceppatelli, M. Pagliai, R. Bini, H. J. Jodl, *J. Phys. Chem. C* **2015**, *119*, 130–140.
- [21] M. Ceppatelli, D. Scelta, M. Serrano-Ruiz, K. Dziubek, G. Garbarino, J. Jacobs, M. Mezouar, R. Bini, M. Peruzzini, *Nat. Commun.* **2020**, *11*, 6125.
- [22] M. Miao, Y. Sun, E. Zurek, H. Lin, *Nat. Rev. Chem.* **2020**, *4*, 508–527.
- [23] M. I. Eremets, A. G. Gavriluk, I. A. Trojan, D. A. Dzivenko, R. Boehler, *Nat. Mater.* **2004**, *3*, 558–563.
- [24] D. Laniel, B. Winkler, T. Fedotenko, A. Pakhomova, S. Chariton, V. Milman, V. Prakapenka, L. Dubrovinsky, N. Dubrovinskaia, *Phys. Rev. Lett.* **2020**, *124*, 216001.
- [25] C. Ji, A. A. Adeleke, L. Yang, B. Wan, H. Gou, Y. Yao, B. Li, Y. Meng, J. S. Smith, V. B. Prakapenka, W. Liu, G. Shen, W. L. Mao, H.-k. Mao, *Sci. Adv.* **2020**, *6*, eaba9206.
- [26] D. Laniel, G. Weck, G. GaiFFE, G. Garbarino, P. Loubeyre, *J. Phys. Chem. Lett.* **2018**, *9*, 1600–1604.
- [27] M. Bykov, T. Fedotenko, S. Chariton, D. Laniel, K. Glazyrin, M. Hanfland, J. S. Smith, V. B. Prakapenka, M. F. Mahmood, A. F. Goncharov, A. V. Ponomareva, F. Tasnádi, A. I. Abrikosov, T. Bin Masood, I. Hotz, A. N. Rudenko, M. I. Katsnelson, N. Dubrovinskaia, L. Dubrovinsky, I. A. Abrikosov, *Phys. Rev. Lett.* **2021**, *126*, 175501.
- [28] W. Sun, S. T. Dacek, S. P. Ong, G. Hautier, A. Jain, W. D. Richards, A. C. Gamst, K. A. Persson, G. Ceder, *Sci. Adv.* **2016**, *2*, e1600225.
- [29] D. Scelta, A. Baldassarre, M. Serrano-Ruiz, K. Dziubek, A. B. Cairns, M. Peruzzini, R. Bini, M. Ceppatelli, *Chem. Commun.* **2018**, *54*, 10554–10557.
- [30] H. J. Beister, K. Strössner, K. Syassen, *Phys. Rev. B* **1990**, *41*, 5535–5543.
- [31] T. Kikegawa, H. Iwasaki, *J. Phys. Soc. Jpn.* **1987**, *56*, 3417–3420.
- [32] R. G. Greene, H. Luo, A. L. Ruoff, *Phys. Rev. B* **1995**, *51*, 597–600.
- [33] O. Degtyareva, M. I. McMahon, R. J. Nelmes, *High Press. Res.* **2004**, *24*, 319–356.
- [34] A. F. Goncharov, E. Gregoryanz, H.-k. Mao, Z. Liu, R. J. Hemley, *Phys. Rev. Lett.* **2000**, *85*, 1262–1265.
- [35] E. Gregoryanz, A. F. Goncharov, C. Sanloup, M. Somayazulu, H.-K. Mao, R. J. Hemley, *J. Chem. Phys.* **2007**, *126*, 184505.
- [36] D. Tomasino, Z. Jenei, W. Evans, C.-S. Yoo, *J. Chem. Phys.* **2014**, *140*, 244510.
- [37] D. Laniel, G. Geneste, G. Weck, M. Mezouar, P. Loubeyre, *Phys. Rev. Lett.* **2019**, *122*, 066001.
- [38] M.-Y. Liu, Y. Huang, Q.-Y. Chen, C. Cao, Y. He, *Sci. Rep.* **2016**, *6*, 29114.
- [39] P. Liu, Y. Zhuang Nie, Q. Lin Xia, G. Hua Guo, *Phys. Lett. A* **2017**, *381*, 1102–1106.
- [40] Y. Hu, T. Shu, C. Mao, L. Xue, Z. Yan, Y. Wu, *Physica B* **2019**, *553*, 195–201.
- [41] J. Zhao, Z.-H. Qi, Y. Xu, J. Dai, X. C. Zeng, W. Guo, J. Ma, *Wiley Interdiscip. Rev.: Comput. Mol. Sci.* **2019**, *9*, e1387.
- [42] Y. Sun, D. Wang, Z. Shuai, *J. Phys. Chem. C* **2017**, *121*, 19080–19086.
- [43] H. Olijnyk, *J. Chem. Phys.* **1990**, *93*, 8968–8972.
- [44] R. L. Mills, B. Olinger, T. D. Cromer, *J. Chem. Phys.* **1986**, *84*, 2837–2845.
- [45] Y. Akahama, K. Kamiue, N. Okawa, S. Kawaguchi, N. Hirao, Y. Ohishi, *J. Appl. Phys.* **2021**, *129*, 025901.
- [46] J. M. Van Den Berg, *Acta Crystallogr.* **1966**, *20*, 905–910.
- [47] C. P. J. M. Van Der Vorst, G. C. Verschoor, W. J. A. Maaskant, *Acta Crystallogr. Sect. B* **1978**, *34*, 3333–3335.
- [48] C. Van der Vorst, W. Maaskant, *J. Solid State Chem.* **1980**, *34*, 301–313.
- [49] W. J. A. Maaskant, *J. Phys. Condens. Matter* **1997**, *9*, 9759–9783.
- [50] J. Breternitz, R. Gunder, H. Hempel, S. Binet, I. Ahmet, S. Schorr, *Inorg. Chem.* **2017**, *56*, 11455–11457.
- [51] M. L. Fornasini, F. Merlo, *Acta Crystallogr. Sect. B* **1976**, *32*, 1864–1867.
- [52] B. Closset, H. Dugas, M. Pegguleryuz, J. E. Gruzleski, *Metal. Trans. A* **1986**, *17*, 1250–1253.
- [53] F. H. Allen, D. G. Watson, L. Brammer, A. Orpen, R. Taylor in *Typical interatomic distances: organic compounds*, in *International Tables for Crystallography, Vol. C*, 3rd Edition, Mathematical, Physical and Chemical Tables (Ed.: E. Prince), Kluwer Academic Publishers, Dordrecht, **2004**, pp. 790–811.
- [54] D. Shriver, M. Weller, T. Overton, J. Rourke, F. Armstrong, *Inorganic Chemistry*, W. H. Freeman, 6th ed., **2014**.
- [55] J. R. Reimers, L. K. McKemmish, R. H. McKenzie, N. S. Hush, *Phys. Chem. Chem. Phys.* **2015**, *17*, 24618–24640.
- [56] J. Weiss, W. Eisenhuth, *Z. Anorg. Allg. Chem.* **1967**, *350*, 9–17.
- [57] K. von Deuten, H. Müller, G. Klar, *Cryst. Struct. Commun.* **1980**, *9*, 1081–1088.
- [58] X. Wang, K. Bao, F. Tian, X. Meng, C. Chen, B. Dong, D. Li, B. Liu, T. Cui, *J. Chem. Phys.* **2010**, *133*, 044512.
- [59] A. Lobato, H. H. Osman, M. A. Salvadó, M. Taravillo, V. G. Baonza, J. M. Recio, *Phys. Chem. Chem. Phys.* **2019**, *21*, 12585–12596.
- [60] K. Tolborg, C. Gatti, B. B. Iversen, *IUCrJ* **2020**, *7*, 480–489.
- [61] J. M. Skelton, L. A. Burton, F. Oba, A. Walsh, *J. Phys. Chem. C* **2017**, *121*, 6446–6454.
- [62] J. M. Skelton, L. A. Burton, F. Oba, A. Walsh, *APL Mater.* **2017**, *5*, 036101.
- [63] A. Walsh, D. J. Payne, R. G. Egdell, G. W. Watson, *Chem. Soc. Rev.* **2011**, *40*, 4455–4463.
- [64] M. D. Nielsen, V. Ozolins, J. P. Heremans, *Energy Environ. Sci.* **2013**, *6*, 570–578.
- [65] C. Chang, L.-D. Zhao, *Mater. Today Phys.* **2018**, *4*, 50–57.
- [66] E. B. Isaacs, G. M. Lu, C. Wolverton, *J. Phys. Chem. Lett.* **2020**, *11*, 5577–5583.
- [67] H. Kim, G. Park, S. Park, W. Kim, *ACS Nano* **2021**, *15*, 2182–2196.
- [68] G. Tan, L.-D. Zhao, M. G. Kanatzidis, *Chem. Rev.* **2016**, *116*, 12123–12149.
- [69] W. G. Zeier, A. Zevalkink, Z. M. Gibbs, G. Hautier, M. G. Kanatzidis, G. J. Snyder, *Angew. Chem. Int. Ed.* **2016**, *55*, 6826–6841; *Angew. Chem.* **2016**, *128*, 6938–6954.
- [70] M. N. Hasan, H. Wahid, N. Nayan, M. S. Mohamed Ali, *Int. J. Energy Res.* **2020**, *44*, 6170–6222.
- [71] Y. Liu, M. Ibáñez, *Science* **2021**, *371*, 678–679.
- [72] D. Scelta, A. Baldassarre, M. Serrano-Ruiz, K. Dziubek, A. B. Cairns, M. Peruzzini, R. Bini, M. Ceppatelli, *Angew. Chem. Int. Ed.* **2017**, *56*, 14135–14140; *Angew. Chem.* **2017**, *129*, 14323–14328.
- [73] Deposition Numbers 2115952, 2115953, 2115954, 2115955, 2115956 contain the supplementary crystallographic data for this paper. These data are provided free of charge by the joint Cambridge Crystallographic Data Centre and Fachinformationszentrum Karlsruhe Access Structures service [www.ccdc.cam.ac.uk/structures](http://www.ccdc.cam.ac.uk/structures).

Manuscript received: October 25, 2021

Accepted manuscript online: November 19, 2021

Version of record online: December 21, 2021